Chinese Chemical Letters 35 (2024) 109526

Contents lists available at ScienceDirect

Chinese Chemical Letters

journal homepage: www.elsevier.com/locate/cclet

Cationic surface polarization centers on ionic carbon nitride for efficient solar-driven H_2O_2 production and pollutant abatement

Zhenyu Hu[1], Zhenchun Yang[1], Shiqi Zeng, Kun Wang, Lina Li, Chun Hu, Yubao Zhao*

MOE Key Laboratory for Water Quality and Conservation of the Pearl River Delta; Institute of Environmental Research at Greater Bay, Guangzhou University, Guangzhou 510006, China

ARTICLE INFO

Article history:
Received 11 October 2023
Revised 26 December 2023
Accepted 12 January 2024
Available online 21 January 2024

Keywords:
Local polarization
Oxygen reduction reaction
Hydrogen peroxide production
Pollutant degradation
Polymeric carbon nitride

ABSTRACT

Solar-driven H_2O_2 production and emerging organic pollutants (EOPs) elimination are of great significance from the perspective of environmental sustainability. The efficiency of the photocatalytic reaction system is the key challenge to be addressed. In this work, the strategy of constructing surface ionic local polarization centers to enhance the exciton dissociation of the polymeric photocatalytic is demonstrated. Selected bipyridinium cation (TMAP) is complexed on a K^+-incorporated carbon nitride (CNK) framework, and the combination of local polarization centers both on the surface (bipyridinium cation) and bulk (K^+ cation) contributes to a superior photocatalytic H_2O_2 production performance, affording a remarkable H_2O_2 generation rate of 46.8 μmol h^{-1} mg^{-1} and a high apparent quantum yield (AQY) value of 77.5% under irradiation of 405 nm photons. As substantiated experimentally by steady state/transient spectroscopy techniques, the surface local polarization centers increase the population of the long-lived trapped electrons, and thereby promote the interfacial charge transfer process for chemical conversion reaction. The strategy is potentially applicable to the design of a wide range of efficient solar-to-chemical conversion systems.

Employing the sustainable solar energy is one of the essential approaches towards the low carbon future of the planet [1]. As one of the most important technologies for utilizing the solar energy, heterogeneous photocatalysis has attracted tremendous research interest for solar energy storage and conversion, in which, development of stable and cost-effective photocatalyst with decent solar conversion efficiency owns the priority. Polymeric carbon nitride (PCN) framework has the favorable features of non-toxicity, physiochemical stability, low cost of synthesis, and most importantly, noticeable visible-light response [2,3]. However, as a typical organic framework, PCN has low dielectric permittivity and high singlet exciton Coulombic binding energy; and the excitons are localized in the heptazine unit, and *via* the overlapped molecular orbitals, the polarons are hopping along the direction perpendicular to the heptazine unit in Brownian motion [4]. These unique features result in low exciton dissociation and short charge diffusion length [5,6], leading to low solar-conversion efficiency of the pristine CN framework [7–9]. The energy-downhill cascade electron transfer process is a crucial component of the photo-to-chemical conversion in natural photosynthesis [10–13]. Comparably, in artificial photosynthesis, donor-acceptor (D-A) microstructure is typically designed to induce an internal local electric field, and thereby provide an energetically downward process for driving the spatial-separation of the charges [14–18]. It is reported that generation of charged/neutral local polarization sites in conjugated polymer could significantly enhance the exciton dissociation [19–23]. Moreover, incorporation of metal ion into the conjugated polymer framework is proven to be efficient in inducing locally polarized micro-environment and boosting the exciton dissociation [24–29]. However, superbly designed reaction systems with notable apparent quantum yields that were created by inducing an internal electric field within a polymeric photocatalyst are occasionally reported, and further breakthrough based on this strategy is highly desired [25,30,31].

Photocatalytic H_2O_2 production is one of the major approaches for solar-to-chemical conversion. Hydrogen peroxide is a versatile chemical, and finds applications in a wide range of areas, such as environmental remediation, energy storage/conversion, and chemical industry [32–35]. Development of the solar-driven H_2O_2 production process is potentially a highly sustainable and cost-effective approach, as compared to the energy-intensive industrial anthraquinone process. Heterogeneous photocatalytic H_2O_2 gener-

* Corresponding author.
E-mail address: ybzhao@gzhu.edu.cn (Y. Zhao).
[1] These authors contributed equally to this work.

https://doi.org/10.1016/j.cclet.2024.109526
1001-8417/

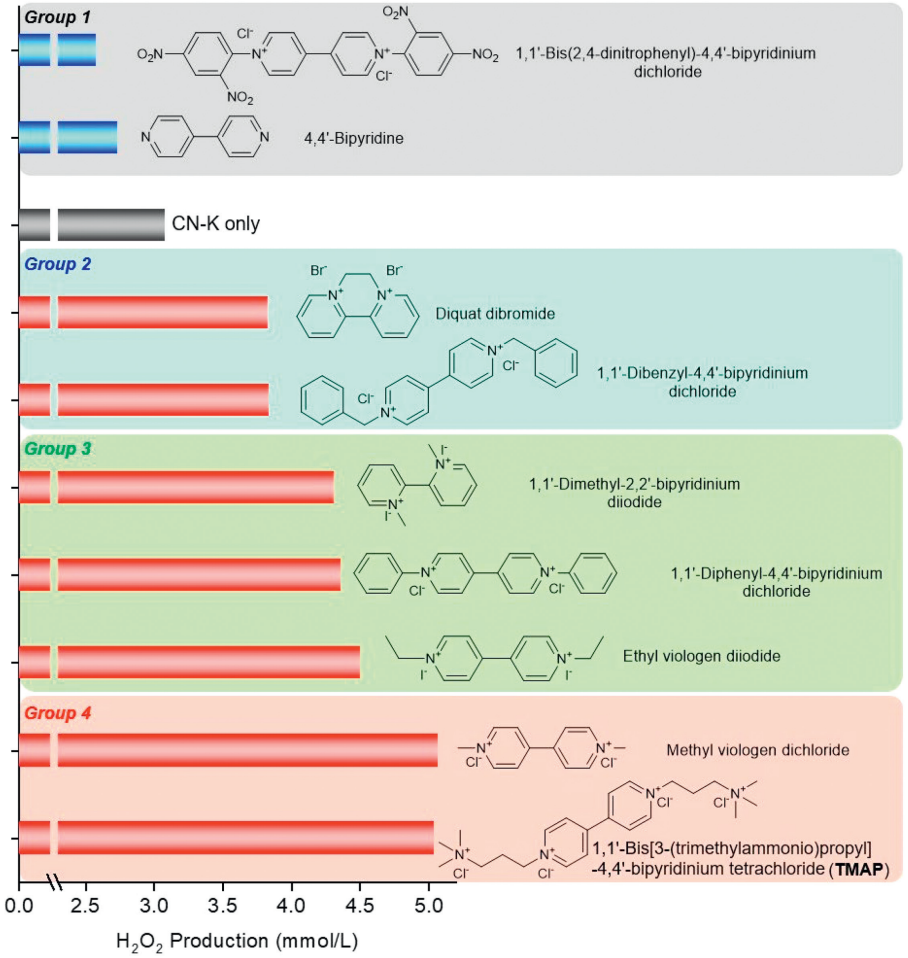

Fig. 1. Photocatalytic H_2O_2 production performance of CNK in the presence of a series of pyridinium ions with various electron withdrawing and electron donating groups for the formation of surface polarization sites. Reaction conditions: 10 mg CNK in 35 mL of aqueous solution of ethanol (5% v/v) in the presence of 10.0 μmol/L pyridinium ions if any; light source, solar simulation with 420 nm band-pass filter and the light intensity was 25 mW/cm^2.

ation *via* selective dioxygen reduction reaction (ORR) exhibits significant environmental-friendliness and sustainability, and is thus attracted enormous research interests [35–37]. Selective 2e$^-$ ORR to H_2O_2 generation is especially favorable in the carbon-centered surface-active sites, and polymeric carbon nitride framework is thereby an ideal platform for realizing efficient solar-driven H_2O_2 production [38–42]. It is thus especially promising to reach a satisfactory efficiency in solar-driven H_2O_2 production by developing novel strategies for upgrading the configuration of the carbon nitride photocatalyzed reaction system.

Herein, we create the combination of pyridinium ion sites induced local polarization on the surface and K^+-complexation caused local polarization in the bulk in a polymeric carbon nitride framework, and demonstrate the remarkable enhancement of the photocatalytic performance by combined local polarizations both in the bulk and on the surface. A trace amount of ionic sites on the surface is essential to the enhancement of the photocatalytic performance: 77.5% apparent quantum yield (AQY) for H_2O_2 production with ethanol as the proton/electron donor. Additionally, some pervasively detected endocrine disruptors and antibiotics could serve as proton/electron donor, and simultaneous H_2O_2 production and emerging organic pollutants degradation is thereby realized.

The K^+-incorporated polymeric carbon nitride framework (CNK) was synthesized *via* a modified method previously reported [43]. In a typical synthesis, 20 g KCl and 10 g melamine were mixed in 100 mL DI water. The mixture was magnetically stirred at 80 °C until all the solvent evaporated. The solid was pulverized and transferred to a 50 mL crucible with a lid. The thermal polymerization was conducted in a maffle furnace at 600 °C for 2 h, and the temperature ramping rate was 5.5 °C/min. After removing the salt by water, CNK was collected and dried at 60 °C in a vacuum oven.

10 mg of photocatalyst was dispersed in 35 mL water with 50 μmol/L EOPs under ultrasonication. The concentration of 1,1′-bis[3-(trimethylammonio)propyl]−4,4′-bipyridinium (TMAP) was 10 μmol/L. The suspension was saturated with O_2 and was then subjected to 420 nm irradiation with light intensity of 25 mW/cm^2. The suspension was sampled at specified time interval, and the aliquot was filtered for collecting the filtrate. The concentration of the hydrogen peroxide in the filtrate was determined by DPD/POD method reported elsewhere [44].

The ionic polymeric CNK is efficient in solar-driven 2e$^-$ ORR for H_2O_2 production, and 30 min photocatalytic reaction generates 3.1 mmol/L H_2O_2, as shown in Fig. 1. For construction of the surface complexed ionic polarization sites, a series of pyridinium ions with various electron-donating and electron-withdrawing functional groups are examined in the photocatalytic H_2O_2 production reaction, so as to correlate the structural features in molecular level with the photocatalytic performances of the complex reaction systems. Based on the intensity of the pyridinium ions for impacting the catalytic performance of CNK in H_2O_2 photo-production, the pyridinium ions were roughly classified into 5 groups (Fig. 2).

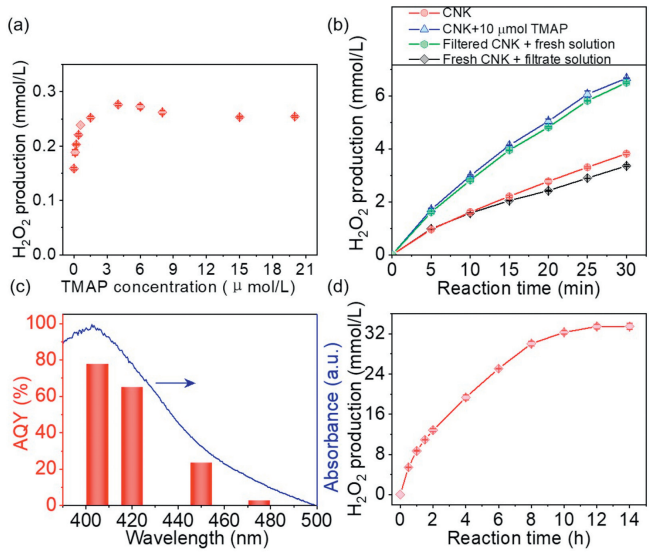

Fig. 2. (a) Photo-production of H_2O_2 as a function of the concentration of 1,1′-bis[3-(trimethylammonio)propyl]−4,4′-bipyridinium (TMAP) cations. (b) Exploration of the role of surface-complexed TMAP for boosting the photocatalytic H_2O_2 production (See Supporting information for experimental details). (c) Apparent quantum yield of the TMAP/CNK photocatalyzed reaction system for H_2O_2 photo-production *via* $2e^-$ ORR. (d) Long-term running performance of TMAP-CNK photocatalytic reaction system. Detailed reaction condition is in the Experimental Section in Supporting information.

As shown in Fig. 1, bipyridine molecule and the bipyridinium ions with strong electron withdrawing nitro-group obviously impede the photocatalytic performance of CNK. In contrast, the diquat cation and 1,1′-dibenzyl-4,4′-bipyridium cation have the similar impact on the enhancement of the photocatalytic performance of CNK, affording 3.8 mmol/L H_2O_2 in 30 min photo-reaction. The bipyridinium ions in Group 3 pose stronger impact on the photocatalytic performance of CNK than the cations in Group 2, and 30 min photo-reaction could generate around 4.4 mmol/L H_2O_2. Among the tested ionic compounds, methyl viologen and TMAP cations show the highest capacity in boosting the catalytic performance of CNK in photocatalytic H_2O_2 production, the H_2O_2 concentration after 30 min photo-irradiation could reach a high value of around 5.0 mmol/L. A survey on the photocatalytic performance of CNK in the presence of various bipyridinium ions reveals the dependence of the photocatalytic activity on the molecular configuration of pyridinium ions; roughly speaking, the electron-richness of the pyridinium ion is beneficial to an efficient photocatalytic performance of CNK.

For further exploring the rationale behind the enhancement of the catalytic performance of CNK, the following experimental investigations were conducted in the optimum reaction system, that is TMAP-CNK. As shown in Fig. 2a, photo-production of H_2O_2 increases with TMAP concentration and then reaches a plateau after a very low TMAP concentration of 4 μmol/L, revealing the powerful impact of TMAP on the photocatalytic behavior of CNK in $2e^-$ ORR. TMAP is inactive under visible light irradiation for photocatalytic H_2O_2 production (Fig. S1 in Supporting information). Further investigation was focused on whether the surface complexed TMAP or the free TMAP in the solution that is contributing positively to the enhancement of the photocatalytic performance. As shown in Fig. 2b, with CNK as the photocatalyst, [H_2O_2] reaches 3.8 mmol/L after a 30 min light irradiation. While in the reaction system with coexisting of 10 μmol/L TMAP and CNK, H_2O_2 concentration reaches 6.7 mmol/L, corresponding to a H_2O_2 production rate of 46.8 μmol per milligram catalyst in 1 h (μmol h^{-1} mg^{-1}). Then, a freshly prepared suspension with CNK and 10 μmol/L TMAP was keep in dark for 1 h to reach adsorption equilibrium; the solid photocatalyst and the solution was then separated by filtration. The filtered solid photocatalyst was then dispersed in a fresh aqueous solution with 5.0% v/v ethanol, and 30 min light irradiation on this reaction system affords 6.5 mmol/L H_2O_2, which is close to that in the reaction system of fresh CNK + 10 μmol/L TMAP. In contrast, the reaction system with the filtrate and fresh CNK produce 3.4 mmol/L H_2O_2, which is close to the reaction system with CNK only. These experiments reveal that enhanced photocatalytic performance of the reaction system is attributed to the CNK with surface complexed TMAP. Additionally, the ionic feature of CNK is important, as the TMAP can only slightly improve the performance of the ion-free neutral carbon nitride (CN) framework (Fig. S2 in Supporting information).

The stability of H_2O_2 in the photocatalytic reaction system is measured, and 1 h photocatalytic reaction in the presence of CNK results in the deposition of 10% of H_2O_2 (Fig. S3 in Supporting information). It is interesting that H_2O_2 decomposition is attenuated by the formation of surface ionic local polarization sites on CNK, and there is only 5% of H_2O_2 decomposed in TMAP-CNK photocatalyzed reaction system after 1 h light irradiation. Attenuated H_2O_2 decomposition is favorable for the accumulation of H_2O_2 in the reaction system. The AQY was measured for evaluating the efficiency of the photocatalytic reaction system under the monochromatic irradiation. As shown in Fig. 2c, the reaction system of TMAP-CNK afford a remarkable AQY of 77.5% and 64.9% at the wavelength of 405 and 420 nm, respectively, demonstrating the powerful capacity of the ionic interaction within the surface-complex of TMAP-CNK in enhancing the photon-to-chemical conversion performance. The performance of TMAP-CNK system was then measured for a prolonged irradiation, and a high H_2O_2 concentration of 33.2 mmol/L was achieved after 12 h of light irradiation (Fig. 2d).

With some of selected EOPs as the electron/proton donor, CNK and TMAP-CNK were employed as the photocatalysts for simultaneous EOPs degradation and H_2O_2 production (Fig. 3). As shown in Figs. 3a2 and a3 and Fig. S4 (Supporting information), in TMPA-CNK photocatalyzed reaction system, BPA, an endocrine disruptor pervasively detected in aquatic environment, could be eliminated within 60 min, while there are 20.9% BPA residual in the CNK photocatalyzed reaction system. Consistently, the concentrations of H_2O_2 were 153.7 μmol/L and 91.7 μmol/L, respectively, in TMAP-CNK and CNK photocatalyzed reaction systems. Similarly, TMAP-CNK shows significantly higher catalytic performance in terms of H_2O_2 generation and antibiotics degradation. Particularly, in the case with sulfamethoxazole as the electron/proton donor (Fig. 3c), 30 min photocatalytic reaction with TMAP-CNK generated 82.9 μmol/L H_2O_2, which is nearly 4 times of that in the CNK photocatalyzed reaction system. In the cases with tetracycline and oxytetracycline as the target pollutants, the degradation rates of the antibiotics are very close, while the obvious distinctions in H_2O_2 generation are speaking repeatedly for the essential contribution of the surface-complexed TMAP to the enhancement of photon-to-chemical conversion efficiency.

We then attempted to explore the rationale behind the enhancement of photocatalytic performance by the surface-complexed ionic local polarization sites. TMAP-CNK was prepared by filtration of the aqueous suspension with CNK and 10 μmol/L TMAP, followed by drying in a vacuum oven. X-ray photoelectron spectroscopy (XPS) analysis on samples of TMAP-CNK and CNK reveals that the amount of TMAP complexed on the surface of CNK is too low to be detected by XPS (Fig. S5 in Supporting information). The following compassion of TMAP-CNK and CNK *via* Fourier transform infrared spectroscopy (FT-IR) also shows no detectable differences (Fig. S6 in Supporting information). Moreover, the formation of surface ionic local polarization sites poses no impact on the layer stacking structure of CNK, as evidenced by the X-ray

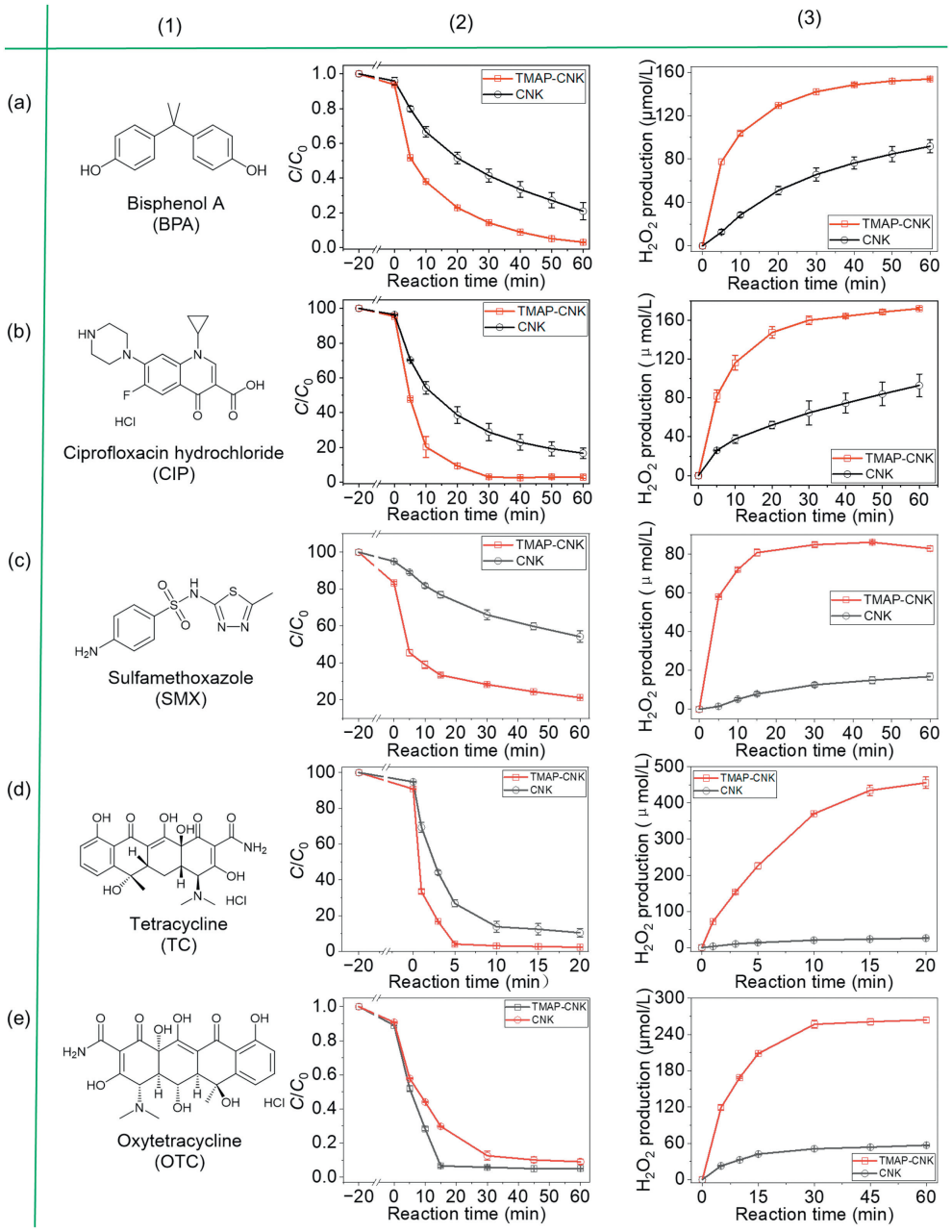

Fig. 3. Photocatalytic H_2O_2 production and degradation of bisphenol A (Row a), ciprofloxacin (Row b), sulfamethoxazole (Row c), tetracycline (Row d), and oxytetracycline (Row e). Molecular structure of the EOPs (Column 1), comparison of TMAP-CNK and CNK in photocatalytic degradation of EOPs (Column 2) and H_2O_2 photo-production (Column 3). Reaction conditions: 10 mg CNK in 35 mL aqueous solution in the presence of 10 μmol/L TMAP; pollutants concentration: 50 μmol/L; light source, solar simulation with 420 nm band-pass filter and the light intensity was 25 mW/cm^2.

diffraction patterns of CNK and TMAP-CNK (Fig. S7 in Supporting information). We then focused on the impact of the low amount of surface complexed TMAP on the photophysical properties of samples. First, the UV–vis spectroscopy was employed for detecting the impact of the local polarization sites on the photon absorption properties of the samples. As shown in Fig. 4a, after the formation of surface ionic local polarization sites, the absorption of TMAP-CNK is more intensive than that of CNK, but the absorption edge is not impacted. An enhanced photon absorption is a favorable feature as it is the initial step of photocatalysis and is fuelling the whole chemical/energy conversion process. Moreover, by XPS, valence band position of evidenced to be the same for both CNK and TMAP-CNK.

After photon absorption, part of the excited states could relax to the ground state *via* photoluminescence (PL), while the other excited states will transit to non-emissive state *via* charge trapping [45]. We thus performed steady-state and transient PL spectroscopy for evaluating the situation of the trapped charges [46]. As shown in Fig. 4b, CNK shows a strong PL emission peak at 470 nm. It is noteworthy that the intensity of PL emission peak decreases with the amount of TMAP on the surface of CNK, demonstrating the contribution of surface ionic local polarization site on attenuation of the emissive decay of the excited states. Together with the DRS analysis, a combined enhanced photon absorption and decreased emissive decay of TMAP-CNK collectively results in higher amount of non-emissive state in TMAP-CNK than in CNK framework. For further understanding the behavior of the emissive decay process, time-resolved PL spectroscopy was employed for analyzing the decay kinetics, and the lifetime of the emissive decay was determined to be 4.9 ns and 4.1 ns for CNK and TMAP-

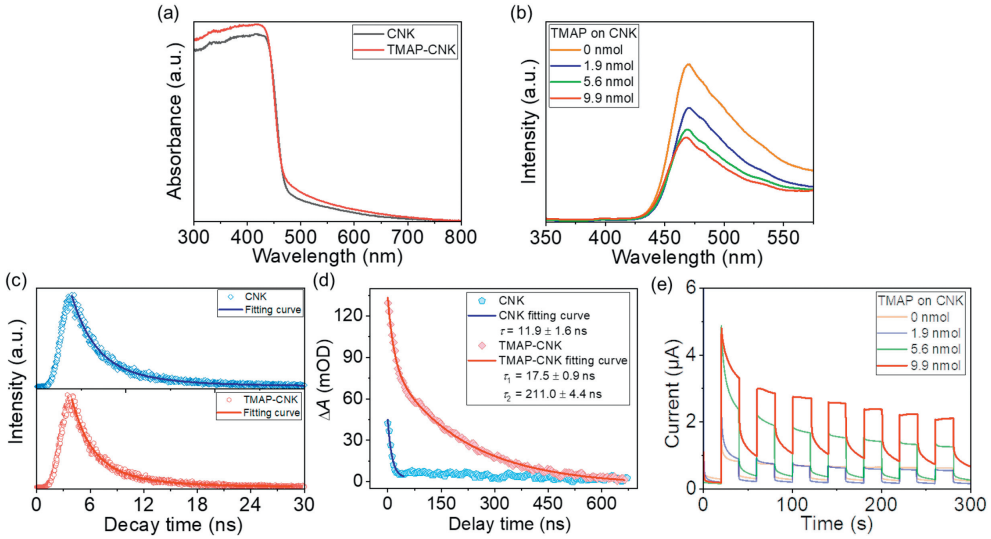

Fig. 4. (a) Diffuse reflectance spectra of the CNK and TMAP-CNK. (b) Steady-state photoluminance spectroscopy of CNK with various amount of TMAP complexed on the surface. Materials preparation: a specific amount of TMAP was loaded on 300 mg of CNK *via* wet impregnation method, and 9.9 nmol TMAP on 300 mg CNK is corresponding to the sample denoted by TMAP-CNK. (c) Transient photoluminance spectroscopy of CNK and TMAP-CNK. (d) Transient absorption spectroscopy of TMAP-CNK and CNK in ns–μs time scale. (e) Photocurrent of CNK with various amount of surface complexed TMAP.

CNK, respectively (Fig. 4c). The shortened PL emission lifetime and lowered PL emission intensity of TMAP-CNK as compare to those of CNK demonstrate fast quenching of the luminescence and reduced exciton recombination resulting from the formation of local polarization sites [47,48].

It is the non-emissive trapped electrons that are potentially capable of initiating the interfacial charge transfer reaction after diffusing to the surface of the photocatalyst. Quantitative analysis on the population and decay kinetics of non-emissive trapped electrons in the presence of surface adsorbed dioxygen was then analyzed by a transient absorption spectroscopy (TAS). As shown in Fig. 4d, the amplitude of TAS signal of TMAP-CNK could reach a high value of 132 mOD, which is roughly 3 times of that in the spectra of CNK (44 mOD), which is consistent with the DRS analysis and demonstrates a higher population of the excited states in TMAP-CNK than in CNK. Moreover, the lifetime of the trapped electron in CNK is around 11.9 ns, while trapped electrons in TMAP-CNK lasts much longer than that in CNK, presenting lifetime of 17.5 ns in the first stage and 211.0 ns in the second stage. The long-lived electrons in the TMAP-CNK are capable of diffusing to the surface and initiating the chemical conversion reaction, and thereby contributing to an enhanced photocatalytic performance in $2e^-$ ORR. For further evaluating the impact of the surface ionic local polarization sites on the charge separation, the photocurrent measurement was performed in a three-electrode photochemical cell. Fig. 4e shows obviously increase of the photocurrent with the amount of TMAP on CNK, revealing that the presence of surface polarization sites could finally results in higher amount of electrons that could reach the surface for chemical conversion reactions.

The reaction mechanism of the photocatalytic O_2 reduction for H_2O_2 production was tentatively explored by a series of quenching reaction and spectroscopic analysis. Firstly, the impact of the atmosphere on the H_2O_2 photo-production was analyzed. As shown in Fig. 5a, under oxygen atmosphere, TMAP-CNK photocatalyzed reaction generates 10.2 mmol/L H_2O_2 in 1 h; while in the air atmosphere, H_2O_2 production decreases to 7.7 mmol/L under the otherwise same reaction condition. There is only 0.4 mmol/L of H_2O_2 generated under N_2 atmosphere, which may result from the reduction of the residue O_2 in the suspension. These experiments demonstrate the critical role of oxygen as the source for H_2O_2

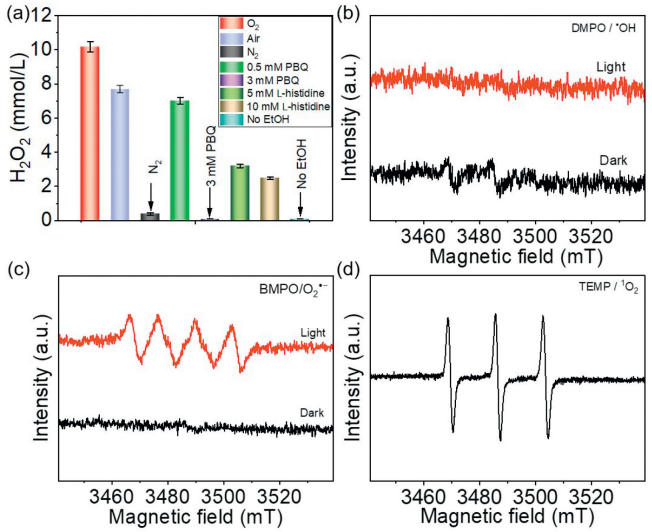

Fig. 5. (a) Quenching experiments in the TMAP-CNK photocatalyzed $2e^-$ ORR. mM is mmol/L. (b) Electron spin resonance spectra with 5,5-dimethyl-1-pyrroline *N*-Oxide (DMPO) as the spin-trapping agent for probing the hydroxyl radical. (c) Electron spin resonance spectra with 5–*tert*-butoxycarbonyl-5-methyl-1-pyrroline-*N*-oxide (BMPO) as the spin-trapping agent for detecting superoxide radical. (d) Electron spin resonance spectra with 2,2,6,6-tetramethylpiperidine (TEMP) as the spin-trapping agent for probing singlet oxygen.

production. Secondly, the generation of H_2O_2 is completely impeded when *para*-benzoquinone, an effective superoxide radical scavenger, is added, proving that the superoxide radical is an important stage during H_2O_2 formation [49]. Thirdly, L-histidine is able be quench the singlet oxygen, and the photocatalytic reaction in the presence of L-histidine generates a low amount of H_2O_2, revealing that the singlet oxygen is one of the critical intermediates during the formation of H_2O_2 [50]. Lastly, the H_2O_2 generation is negligible in the absence of ethanol, demonstrating the critical role of the electron/proton donor (either ethanol or EOPs).

Further probing of the intermediates was performed using electron spin resonance (ESR) spectroscopy. As shown in the ESR spectra collected with spin trapping agent of 5,5-dimethyl-1-pyrroline *N*-oxide (DMPO) for probing hydroxyl radical in aque-

ous system, no obvious resonance signal is observed, indicating that no hydroxyl radical (•OH) forms in the reaction (Fig. 5b). Using 5–*tert*-butoxycarbonyl-5-methyl-1-pyrroline-*N*-oxide (BMPO) as the spin trapping agent, the quartet signal collected by ESR spectrometer, demonstrating the production of superoxide radical ($O_2^{\bullet-}$) under light irradiation (Fig. 5c). Additionally, using 2,2,6,6-tetramethylpiperidine (TEMP) as the spin-trapping agent for probing singlet oxygen, ESR spectrum collected in TMAP-CNK photocatalyzed reaction system presents a characteristic triplet signal of TEMPO, revealing the generation of singlet oxygen ($^1O_2$) (Fig. 5d). The ESR studies are in line with the abovementioned quenching reactions. Based on the mechanistic investigations and the previous reports, it is thus proposed that $O_2^{\bullet-}$ could be oxidatively converted to $^1O_2$, and the following reaction with proton/electron donor (ethanol or EOPs) could generate H_2O_2 [27,51–53].

Targeting on boosting the efficiency of photocatalytic H_2O_2 production to a high level, the strategy of using local polarization induced energetically downhill process to enhance exciton dissociation was developed in this work. On an already highly activity CN with K^+ induced local polarization in the bulk, bipyridinium cation was complexed on the surface for inducing additional surface polarization centers. Due to the combination of polarization centers both in bulk and on surface, the complex photocatalyst of TMAP-CNK exhibited superior photocatalytic performance in selective $2e^-$ ORR for H_2O_2 generation, affording a remarkable AQY of 77.5% with ethanol as the proton/electron donor. A prolonged photocatalytic reaction afforded H_2O_2 with a high concentration of 33.5 mmol/L. The surface-complexed local polarization sites were evidenced to contribute essentially to the enhanced photon absorption, impeded emissive decay, boosted quantity of long-lived non-emissive excited states. All these favorable impacts led to the promotion of the photocatalytic performance in simultaneous photocatalytic H_2O_2 production and EOPs degradation. The conclusion in this work could shed light on the design of highly efficient photocatalysts *via* fabrication of delicate local polarization centers on the surface.

Declaration of competing interest

The authors declare no conflicts of interest.

Acknowledgments

Financial supports by the National Natural Science Foundation of China (No. 21976041), Guangzhou Municipal Science and Technology Project (No. 202201020168), Tertiary Education Scientific Research Project of Guangzhou Municipal Education Bureau (No. 202235238), and Guangdong Basic and Applied Basic Research Foundation (No. 2023A1515010788) are acknowledged.

Supplementary materials

Supplementary material associated with this article can be found, in the online version, at doi:10.1016/j.cclet.2024.109526.

References

[1] F. Chen, Y. Zhang, H. Huang, Chin. Chem. Lett. 34 (2023) 107523.
[2] Q. Wang, G. Zhang, W. Xing, et al., Angew. Chem. Int. Ed. 62 (2023) e202307930.
[3] Q. Deng, H. Li, W. Hu, W. Hou, Angew. Chem. Int. Ed. 62 (2023) e202314213.
[4] C. Merschjann, S. Tschierlei, T. Tyborski, et al., Adv. Mater. 27 (2015) 7993–7999.
[5] C. Sun, Z. Wu, Z. Hu, et al., Energy Environ. Sci. 10 (2017) 1784–1791.
[6] O.V. Mikhnenko, P.W.M. Blom, T.Q. Nguyen, Energy Environ. Sci. 8 (2015) 1867–1888.
[7] H. Wang, S. Jiang, S. Chen, et al., Chem. Sci. 8 (2017) 4087–4092.
[8] H. Wang, X. Sun, D. Li, et al., J. Am. Chem. Soc. 139 (2017) 2468–2473.
[9] A. De Sio, F. Troiani, M. Maiuri, et al., Nat. Commun. 7 (2016) 13742.
[10] T.M. Clarke, J.R. Durrant, Chem. Rev. 110 (2010) 6736–6767.
[11] Y. Wang, A. Vogel, M. Sachs, et al., Nat. Energy 4 (2019) 746–760.
[12] A. Yamakata, M. Yoshida, J. Kubota, M. Osawa, K. Domen, J. Am. Chem. Soc. 133 (2011) 11351–11357.
[13] D. Veldman, Ö. İpek, S.C.J. Meskers, et al., J. Am. Chem. Soc. 130 (2008) 7721–7735.
[14] H. Lin, J. Wang, J. Zhao, et al., Angew. Chem. Int. Ed. 61 (2022) e202117645.
[15] J. Kosco, M. Bidwell, H. Cha, et al., Nat. Mater. 19 (2020) 559–565.
[16] Z.A. Lan, G. Zhang, X. Chen, et al., Angew. Chem. Int. Ed. 58 (2019) 10236–10240.
[17] H. Ou, X. Chen, L. Lin, Y. Fang, X. Wang, Angew. Chem. Int. Ed. 57 (2018) 8729–8733.
[18] Z.A. Lan, M. Wu, Z. Fang, et al., Angew. Chem. Int. Ed. 60 (2021) 16355–16359.
[19] L. Dai, A. Dong, X. Meng, et al., Angew. Chem. Int. Ed. 62 (2023) e202300224.
[20] J. Yang, A. Acharjya, M.Y. Ye, et al., Angew. Chem. Int. Ed. 60 (2021) 19797–19803.
[21] C. Wu, Z. Teng, C. Yang, et al., Adv. Mater. 34 (2022) 2110266.
[22] H. Wang, C. Yang, F. Chen, G. Zheng, Q. Han, Angew. Chem. Int. Ed. 61 (2022) e202202328.
[23] Z. Yu, X. Yue, J. Fan, Q. Xiang, ACS Catal. 12 (2022) 6345–6358.
[24] Y. Zhao, P. Zhang, Z. Yang, et al., Nat. Commun. 12 (2021) 3701.
[25] G. Zhang, L. Lin, G. Li, et al., Angew. Chem. Int. Ed. 57 (2018) 9372–9376.
[26] S. Zeng, L. Li, Z. Yang, et al., J. Phys. Chem. C 126 (2022) 20028–20035.
[27] Z. Yang, L. Li, J. Gao, et al., ACS EST Eng. 2 (2022) 2142–2149.
[28] A. Savateev, N.V. Tarakina, V. Strauss, et al., Angew. Chem. Int. Ed. 59 (2020) 15061–15068.
[29] Z. Teng, Q. Zhang, H. Yang, et al., Nat. Catal. 4 (2021) 374–384.
[30] J. Liu, M. Antonietti, Energy Environ. Sci. 6 (2013) 1486–1493.
[31] Z. Mi, T. Zhou, W. Weng, et al., Angew. Chem. Int. Ed. 60 (2021) 9642–9649.
[32] K. Jiang, S. Back, A.J. Akey, et al., Nat. Commun. 10 (2019) 3997.
[33] P. Zhang, D. Sun, A. Cho, et al., Nat. Commun. 10 (2019) 904.
[34] S.N. Lou, J. Lim, T.H. Jeon, W. Choi, ACS EST Eng. 2 (2022) 1116–1129.
[35] C. Dong, Y. Yang, X. Hu, et al., Nat. Commun. 13 (2022) 4982.
[36] J. Xu, Q. Zhang, X. Gao, et al., Angew. Chem. Int. Ed. 62 (2023) e202307018.
[37] Y. Wu, H. Che, B. Liu, Y. Ao, Small Struct. 4 (2023) 2200371.
[38] Y. Zhao, M. Antonietti, Angew. Chem. Int. Ed. 56 (2017) 9336–9340.
[39] Y. Zhao, M. Shalom, M. Antonietti, Appl. Catal. B 207 (2017) 311–315.
[40] J. Qin, J. Barrio, G. Peng, et al., Nat. Commun. 11 (2020) 4701.
[41] S. Mazzanti, G. Manfredi, A.J. Barker, et al., ACS Catal. 11 (2021) 11109–11116.
[42] P.Y. Zhang, J. Zhang, D.D. Wang, et al., Appl. Catal. B 318 (2022) 121749.
[43] Z. Yang, L. Li, S. Zeng, et al., ACS Appl. Mater. Interfaces 15 (2023) 8232–8240.
[44] G.h. Moon, W. Kim, A.D. Bokare, N.e. Sung, W. Choi, Energy Environ. Sci. 7 (2014) 4023–4028.
[45] K.L. Corp, C.W. Schlenker, J. Am. Chem. Soc. 139 (2017) 7904–7912.
[46] C. Merschjann, T. Tyborski, S. Orthmann, et al., Phys. Rev. B 87 (2013) 205204.
[47] P. Kumar, E. Vahidzadeh, U.K. Thakur, et al., J. Am. Chem. Soc. 141 (2019) 5415–5436.
[48] Q. Liang, Z. Li, Z.H. Huang, F. Kang, Q.H. Yang, Adv. Funct. Mater. 25 (2015) 6885–6892.
[49] M. Hayyan, M.A. Hashim, I.M. AlNashef, Chem. Rev. 116 (2016) 3029–3085.
[50] E.T. Yun, J.H. Lee, J. Kim, H.D. Park, J. Lee, Environ. Sci. Technol. 52 (2018) 7032–7042.
[51] J. Luo, C. Fan, L. Tang, et al., Appl. Catal. B 301 (2022) 120757.
[52] W. Liu, P. Wang, J. Chen, et al., Adv. Funct. Mater. 32 (2022) 2205119.
[53] Z. Yang, L. Li, J. Cui, et al., Chem. Eur. J. 28 (2022) e202202122.